

Trapped Particles in the Reversed Field Pinch

Marco GOBBIN, Luca GUAZZOTTO, Shi Chong GUO, Italo PREDEBON, Fabio SATTIN,
Gianluca SPIZZO, Paolo ZANCA and Susanna CAPPELLO

Consorzio RFX, Associazione Euratom-ENEA sulla Fusione, Padova, Italy

(Received: 26 August 2008 / Accepted: 26 November 2008)

The presence and role of trapped particles in the Reversed Field Pinch (RFP) configuration is considered, with an estimate of their relative population and a description of the characteristic trajectories, in particular for the RFX-mod [1] geometry. The particle's orbit scale lengths (e.g. banana width, mean free path) are classified both for ions and electrons, also in the presence of a background chaotic magnetic field and/or a strong helical modulation of the toroidal equilibrium. The study combines analytical estimates and numerical results obtained with the Hamiltonian guiding center code ORBIT [2] and the equilibrium code FLOW [3]. The impact on particle transport, the origin and the magnitude of the bootstrap current and the amount of the neoclassical correction to the resistivity are investigated, both in axisymmetric and helical geometry.

Keywords: Trapped particles, bootstrap current, neoclassical effects, resistivity, RFP, QSH.

1. Introduction

Particle trapping occurs in magnetic confinement devices due to magnetic field non-uniformities, as a consequence of magnetic moment conservation. Trapped particles are known to have noticeable effects in Tokamaks, e.g. for the development of neoclassical transport and the presence of bootstrap current [4].

In Reversed Field Pinches (RFPs) this issue has been relatively less considered. Investigations from MST team [5] pointed out that, although the fraction of trapped particles is pretty much the same in RFPs and Tokamaks, their contribution to transport is much reduced in the former class of devices. Conversely, numerical simulations of a reactor-grade RFP by Shiina [6] revealed that, under some conditions, trapped particles may be relevant, in particular for the generation of bootstrap current.

The previous investigations were carried out in the axisymmetric Multiple Helicity (MH) state of the RFP, where the plasma, in order to self-sustain the magnetic configuration, develops a multitude of saturated tearing instabilities. The resulting overlapping of magnetic islands leads to magnetic field lines chaos. Recent advances in the external control of magnetic modes have allowed RFPs to access the improved Quasi-Single Helicity (QSH) regime, where one mode dominates over a background of secondary ones. This state preludes to the purer, numerically predicted ([7] and refs. therein), Single Helicity (SH) regime, characterized by negligible secondary mode amplitudes. In such regimes, a central helical core with well conserved magnetic surfaces emerges. The structure winds around the torus with the

pitch of the dominant mode. The chaos-free core is at a substantially higher (\sim twice) temperature than its surroundings. Neoclassical effects on transport are expected to be enhanced there. The synergy between toroidal effects on the magnetic field and the helical structure leads to novel effects, including the emergence of a new class of orbits for trapped particles.

Our goal is to provide a broad coverage of the subject of trapped particles in RFPs, with explicit reference to RFX-mod device [1]. In Sect. 2 we will address the pure axisymmetric case. This is done to provide reference conditions to be compared against equivalent simulations in SH states. The mathematical machinery to deal with toroidally symmetric states is well developed and known; hence, only few details of the calculations need to be provided. Sect. 3 deals with SH-QSH states. The mathematical handling of these topologies is more involved and we resorted to numerical simulations of test particle dynamics.

2. Trapped particles in toroidal axisymmetric RFPs.

Fraction of trapped particles. The fraction of trapped particles in RFPs has only a little difference with respect to that in tokamaks, where the trapped fraction is estimated as $f_t \sim (2\varepsilon)^{1/2}$ ($\varepsilon = r/R \ll 1$, with r and R minor and major radius respectively). In RFPs the poloidal magnetic field B_θ is of the same order as the toroidal magnetic field B_ϕ and the magnetic mirror effect results from both fields.

Different approaches have been used and compared here

author's e-mail: marco.gobbin@igi.cnr.it, susanna.cappello@igi.cnr.it

to calculate the trapped fraction: an analytical one, based on the equilibrium model described in [8, 9], and two numerical ones, based on the perturbative and full axisymmetric equilibrium codes, respectively the RFX equilibrium reconstruction code RFXTOR [11], and the FLOW code [3]. In all of these cases, a Maxwellian distribution of electron velocities has been assumed.

In the analytical model the fields are expressed as: [8,9]:

$$B_\phi = B_{o\phi}(r)(1 - \varepsilon \cos \theta), \quad B_\theta = B_{o\theta}(r)(1 - \Lambda(r) \cos \theta)$$

with

$$\Lambda(r) = \frac{r}{R_o} \left[1 + \frac{8\pi p}{B_{o\theta}^2} - \frac{1}{r^2 B_{o\theta}^2} \int_0^r (16\pi p + B_{o\theta}^2) r dr \right]$$

where $B_{o\theta}, B_{o\phi}$ are the equilibrium solution in cylindrical geometry. To first order in ε , we obtain

$$B = B_{r=0}(1 - \delta(r) \cos \theta), \quad \text{where } B = \sqrt{B_\phi^2 + B_\theta^2}$$

and $\delta(r) = (B_{o\phi}^2 \varepsilon + B_{o\theta}^2 \Lambda) / B_o^2$

Since the trapped particles will be those with energy in the interval $\mu B_o(1 - \delta) < E < \mu B_o(1 + \delta)$, where $E = v_\perp^2 + v_\parallel^2$ and $\mu = v_\perp^2 / B$, the corresponding cone for trapped particles is $v_\parallel / v_\perp \leq \sqrt{2\delta}$. Integration on the particle distribution function over this cone of the velocity space gives the estimate $f_t = \sqrt{2\delta}$. Since in RFPs $\Lambda(r) < \varepsilon$, which yields $\delta < \varepsilon$, the fraction of trapped particles in (toroidal) axisymmetric RFP tends to be smaller than that in tokamak with same aspect ratio ε .

A more precise estimate of trapped particle fraction may be obtained by the formula found in [10], where the fraction is a flux surface function which is expressed by:

$$f_t = 1 - \frac{3}{4} \int_0^{\lambda_c} \lambda \left\langle \sqrt{1 - \lambda \frac{B}{B_o}} \right\rangle^{-1} d\lambda \quad (1)$$

where $\langle \rangle$ denotes the flux surface average, $B_o = \langle B^2 \rangle^{1/2}$, and $\lambda_c = B_o / B_M$, being B_M the maximum of B on a given flux surface. We evaluated f_t from Eq. (1) using RFX-mod edge magnetic measurements as input for the RFXTOR model as described in [11].

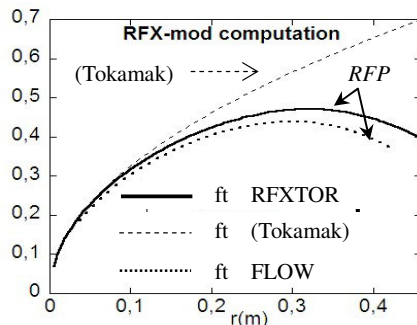


Fig.1 Trapped particles fraction f_t . Solid line: (RFXTOR) RFX-mod MH equilibrium (Eq. 1); (Dashed line: Tokamak with the same aspect ratio); Dotted line: result from FLOW code.

A typical profile for a standard RFX-mod equilibrium at $I_p = 1\text{MA}$ is plotted against the radial coordinate in Fig. 1

(solid line). The result is very close to the analytical estimate discussed above which is not shown in the figure for the sake of clarity.

The FLOW code calculates 2-dimensional equilibria of magnetic confinement devices. It solves a generalized version of the Grad-Shafranov (GS) equation, which includes plasma rotation and reduces to the standard GS in the static case. Only static equilibria are considered here.

In FLOW the magnetic fields are defined by the standard axisymmetric representation: $B_\phi = F(\Psi)/R$, $B_\theta = \nabla\Psi \times \nabla\phi$.

The trapped fraction is given by the expression obtained in Ref. [8b p. 484-485]:

$$f_t(\psi) = \sqrt{1 - B(\psi, \theta = 0) / B_M(\psi)} \quad (2),$$

with ψ magnetic surface label, θ angle along the surface.

The trapped fraction is then computed directly from Eq. (2) for the same RFX-mod equilibrium as above, with central temperature $T = T_i + T_e = 1.6$ keV and flat density profile ($\beta_{pol} = 7\%$). The result is plotted in Fig. 1 (dotted line). We note that spatial profiles for physical quantities which depend on the trapped fraction, e.g. transport coefficients and bootstrap current, must be calculated taking into account the full spatial dependence of the trapped fraction. We further remark that the maximum of f_t does not occur at the plasma edge, as it would be the case for a tokamak: in an RFP f_t is not a monotonic function of radius r .

Bootstrap current and neoclassical resistivity. The bootstrap current J_{BS} is evaluated with the knowledge of temperature and pressure profiles:

$$\langle \mathbf{J}_{BS} \cdot \mathbf{B} \rangle = L_{31} \left[\frac{p'_e}{p_e} + \frac{1}{Z} \left(\frac{p'_e}{p_e} + \alpha \frac{T'_e}{T_e} \right) \right] + L_{32} \frac{T'_e}{T_e} \quad (3)$$

The functions L_{ij} , α , depend on f_t as well as on magnetic equilibrium [12]. The results obtained with the RFX equilibrium model are shown in Fig. 2a (solid line).

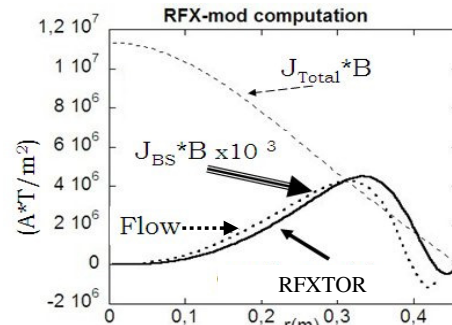


Fig.2-a Bootstrap and total (parallel) current profiles estimated by the models: J_{BS} multiplied by 10^3 .

Similar results are obtained using FLOW based on two formulations similar to Eq. (3), which express the bootstrap current as given in Refs. [13, 14] (Sauter) and [15]

(Houlberg). (The last one is included in the public package named NCLASS). The formulas of the two approaches are obtained either by taking a numerical fit of a series of numerical solutions of the Fokker-Planck equation with the full collision operator [13], or using a Laguerre polynomial expansion for the collision operator [15]. Both of the formulations have been implemented in FLOW and provide nearly identical estimates: in Fig. 2-a, we only plot the Sauter model result (solid line), in order to compare it with the RFXTOR estimate (dotted line). All of the results are found to be in good agreement.

Note that the parallel bootstrap current has a large poloidal component in RFPs. That is again due the toroidal and poloidal fields being of the same order of magnitude.

The unambiguous result, confirming earlier estimates, is that, in present-days RFPs, the bootstrap mechanism can provide only a negligible amount of additional current.

The results of [13-15] can also be used to calculate neoclassical resistivity. Numerical evaluation of neoclassical resistivity has been included in the postprocessing routines of FLOW in the process of evaluating the bootstrap current. The reader is referred to the literature for the details of the models. In the present work, we will only refer to the simplest approach (from the user's point of view): that is, to the Sauter model. In Ref. [13], neoclassical conductivity is expressed with a numerical fit as a function of $f_i^{(eff)}$. For the same standard equilibrium as above the neoclassical resistivity profile shown in Fig. 2-b is obtained. Note that neoclassical resistivity is larger than Spitzer resistivity by a numerical factor going from ~ 1.1 in the center to ~ 2 at the edge consistently with the estimates performed in [16].

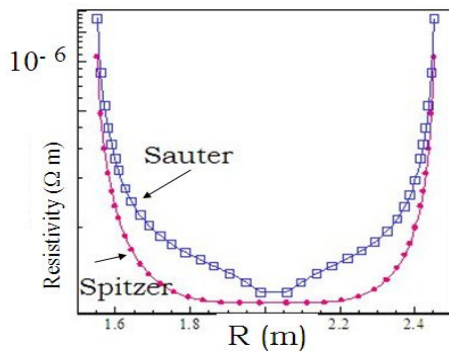


Fig.2-b Neoclassical resistivity profile for an RFX standard equilibrium at $I_p=1$ MA.

Banana orderings with respect to collision and chaotic decorrelation scales. In this paragraph, we provide more details about the ordering of the main parameters of a banana orbit, namely its width on the mid-plane and the bounce time (τ_{bounce} , the period of a complete banana orbit), with respect to collisions and chaotic correlation time (in MH state). To perform these calculations, we will make use of the Hamiltonian guiding

centre code ORBIT [2]; we will normalize all times to the toroidal transit time on the axis ($\tau_{\text{tor}}=2 \pi R_0/v_{\text{th}}$, with v_{th} the thermal velocity, in RFX-mod $\tau_{\text{tor}} \sim 40\text{-}60 \mu\text{s}$ for protons with $E=250\text{-}500$ eV), and characteristic lengths to one toroidal turn.

The parameters relative to the banana orbit are reported in table I for H-ions deposited with energy 250, 500 and 1 keV at $r=10$ cm and $r=25$ cm respectively (minor radius $a=46$ cm in RFX-mod). The banana width ranges between 0.2 and 1 cm, and is of the same order of the proton gyroradius; in the electron case, with energy $E=1\text{keV}$ it is less than 1mm. Bananas are therefore rather small compared to that in Tokamak.

The bounce time depends on the initial pitch of the particle: a minimum value is obtained for particles deposited with zero normalized parallel velocity (i.e. with particle pitch $\lambda=v_{\parallel}/v=0$), and goes to infinity for particles at the trapped-passing boundary. To get reference values, one can consider particles that perform a banana orbit $\approx 180^\circ$ wide poloidally. The resulting values at different radii, typically $\tau_{\text{bounce}}/\tau_{\text{tor}} \sim 1$, are found in table I.

Proton energy (eV)	Bounce time/ τ_{tor} $r=10\text{cm}$	Banana width (cm), $r=10$ cm	Bounce time, / τ_{tor} $r=25$ cm	Banana width (cm), $r=25\text{cm}$	Gyro-Radiu s (cm) $r=a$
250	0.94-1.2	0.5	0.77-0.86	0.2	0.5
500	0.94-1.2	0.7	0.77-0.86	0.3	0.75
1000	0.94-1.2	1.0	0.77-0.86	0.4	1.25

Table I: bounce time (normalized to one toroidal transit) and banana width for protons deposited at $r=10$ and 25 cm respectively, with energies 0.25, 0.5 and 1 keV. Bounce times refer to protons deposited with $\lambda=v_{\parallel}/v=0$ (minimum value) and for a banana 180° wide on the poloidal plane. Gyroradius is evaluated at $r=a$.

Note that the ratio $\tau_{\text{bounce}}/\tau_{\text{tor}}$ does not depend on proton energy, since it is determined by the ratio between the poloidal and toroidal lengths when the particle follows the field line: an approximate value is given by $\tau_{\text{bounce}} = \sqrt{2R_0/r} q \tau_{\text{tor}}$ [4]. A typical collision time for H ion-ion encounters is one collision per 1 - 20 toroidal transits (thermal ions with energy from 250eV to 1 keV, and density $4 \cdot 10^{19} \text{ m}^{-3}$); therefore, for thermal ions the bounce time is somewhat smaller than the collision time (τ_c), while in high density regimes classical (collisional) transport could overcome neoclassical transport.

A banana orbit, in the MH state, can be modified by magnetic chaos and one might envisage a de-correlation (sort of de-trapping) effect to come into play.

In Fig. 3 the parallel correlation length of the chaotic field is plotted as a function of the magnetic field fluctuation (normalized to the poloidal field at the edge). With typical

fluctuation strength of 4%, the correlation length is about 1.5 toroidal turns, therefore closer to the collision length than to the banana toroidal excursion. To get the correlation length about 0.2 toroidal turns (therefore, comparable to the banana toroidal precession width), we have to increase fluctuations up to 50% of the equilibrium poloidal field, which is rather unrealistic.

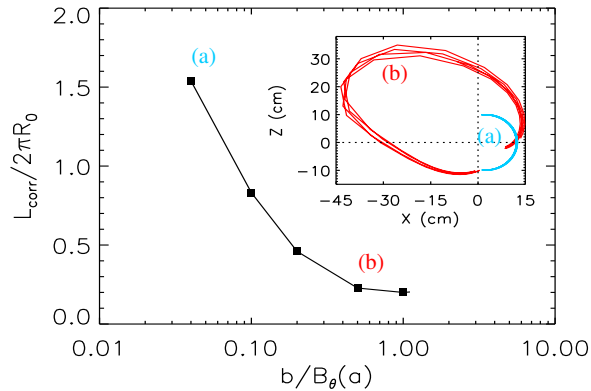


Fig.3 Normalized parallel magnetic correlation length as a function of the normalized mode amplitude. Inserts: banana orbit of a particle deposited at $r=25$ cm, with: $b/B_\theta(\alpha)$ (a) =4% and (b)=50%. Banana orbits are modified by the chaotic field only at very large values of fluctuations. In RFX-mod we expect bananas not to be affected by chaos, even in MH state.

Inserts in Fig. 3 show the poloidal sections of a banana orbit at various fluctuation amplitudes: $b/B_\theta(\alpha)=4\%$ (a) and 50% (b). It is evident that with 4% fluctuations the banana is almost unaffected, while the orbit is significantly deformed only in the case with 50% fluctuations. Trapped particles explore too short a portion of magnetic field line to experience chaos effects.

Summarizing: in the RFP, the proton bounce time is about $2/3$ to 1 toroidal turn; even in the chaotic MH state the banana orbit is not affected by magnetic fluctuations. The typical ordering for protons is: $\tau_{\text{bounce}} = (2/3) \div 1 \times \tau_{\text{tor}} < \tau_{\text{corr}} < \tau_v$, with τ_{corr} the characteristic time to cover the correlation length (with thermal speed). The typical times characterizing particle dynamics in the MH RFP are all of the same order of magnitude, differing by a factor ≈ 2 . In RFX-mod high density regimes, however, the collision time becomes smaller than the others and significant effects can then be expected on transport.

3. Particle dynamics in SH states

Single particle motion. The behavior of particle trapping is deeply modified when the SH configuration of the magnetic field is considered.

In fact, numerical simulations show that the presence of a helical structure increases the fraction of trapped particles

by a factor depending on the SH mode amplitude. A typical experimental helical modulation ($m=1, n=7$) of the order of 3%-6% of the axisymmetric field, enhances the total fraction of trapped particles by 5%-10%.

The helical geometry introduces a new field ripple with respect to the axisymmetric case: as shown in Fig. 4 the variation of $|B|$ experienced by a particle following a single field-line is given by the superposition of a toroidal ripple (slow sinusoidal variation), corresponding to the toroidal geometry, and a helical ripple (faster variation) corresponding to the helical component. As a consequence, two types of trapping are possible; particles can be either localized or blocked, depending on initial position, pitch angle and helical amplitude [17]. The localized - high magnetic moment - particles (trapped in the helical ripple), execute the usual thin banana orbits with a simple toroidal drift across the island, almost insensitive to the helical geometry. The blocked particles (trapped in the toroidal ripple), with a lower magnetic moment, encounter the mirror points along the helical structure after some poloidal turns and have larger radial excursions inside the island itself, thus being subjected to a significant radial transport. These particles can be found throughout the plasma section, but in particular in the exterior region of the island: here the trapped particles can constitute more than one half of the local particle population ($\theta=0$ plane) [18].

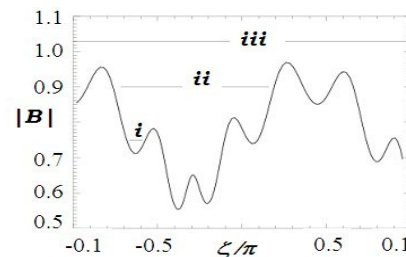


Fig 4: Magnetic field ripple in a SH configuration (initial $\psi_p=0.04$) with the three trapping states: localized (i), blocked (ii) and passing (iii).

The transition between these two trapping states is possible even in absence of collisions, in analogy with the stellarator behavior [19]. Considering all the kind of trapping mechanisms and assuming a uniform deposition of particles only within the helical structure, it has been evaluated that the total fraction of trapped particles achieves the value 40%.

Neoclassical transport in QSH states. The transport resulting from trapped and passing particles in the helical regimes of the RFP has been studied by the Hamiltonian guiding center code ORBIT. To this end a dedicated algorithm has been developed, which is described with details in [20]. It is based on the determination of the helical magnetic flux ψ^M associated to the helical magnetic surfaces reconstructed in RFX-mod QSH

regimes. An example of normalized helical flux contour plot on a poloidal cross section is shown in fig. 5-a. Different temperatures and collisional regimes of the plasma background in the range $T_{e,i} = 300 - 1000 \text{ eV}$ are considered. A set of test particles with random pitch angle λ are deposited inside the helical structure. Following their dynamics, particles are considered lost when they cross a prescribed helical loss surface (black curve in fig. 5-(a)); they are then injected back in the helical axis position, so as to keep constant the particles number during the whole simulation. Test particles are mono-energetic and characterized by the same temperature of the plasma background. Both classical and pitch angle collisions are implemented in the simulations. The first are responsible of a random displacement of the guiding center position of a test particle by a Larmor radius, while the latter changes randomly the pitch angle. Energy is conserved in these collisions and, by changing the pitch angle, a particle can switch from trapped to passing or vice-versa.

Simulations at low plasma temperatures (about 250-300 eV) in *QSH* (both with and without secondary modes) show that the steady-state density of test ions or electrons is linear versus the normalized helical magnetic flux ψ^M , decreasing from a maximum value at the island O-point (source) to zero at the helical loss surface, as seen in Fig.5-b), black line.

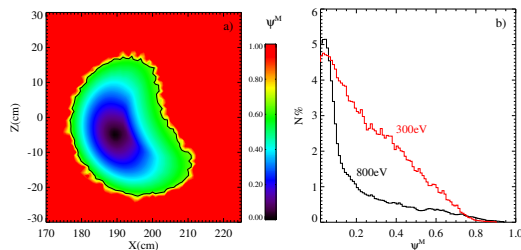


Fig.5 a) Normalized helical flux ψ^M contour plot on a poloidal cross section. The black curve corresponds to the loss helical surface. b) Ion distribution inside the helical structure in a RFX-mod QSH shot for $T = 300\text{eV}$ (red curve) and for $T=800\text{eV}$ (black curve).

A diffusion coefficient D can be estimated as the ratio of the outgoing flux and the density gradient (Fick's law). Typical values of D for low temperature QSH in RFX-mod plasmas have been found to be in the range: $0.1-1 \text{ m}^2/\text{s}$ [21] to be compared with the classical prediction of $0.05-0.1\text{m}^2/\text{s}$. The increase of D is a direct consequence of the enhancements of neoclassical effects within the helical structure mainly due to the larger banana width with respect to a pure axisymmetric case, as will be shown in the following.

Recently thermal measurements performed in the

RFX-mod experiment during QSH states have shown large helical structures, identified by significant temperature gradient in the plasma core, which can reach a considerable size (25-50% of plasma radius) and temporal persistence up to 85% the flat top phase ($\sim 200\text{ms}$) of the discharge. These states are characterized by the separatrix expulsion from the helical core and are named as SHAx regimes (Single Helical Axis, see [22]). Electron temperatures in these plasmas can be of the order of 1keV which corresponds to a very low collisionality. In fact, the collision frequency of the test ions with the background decreases from about 4kHz at 300 eV to 0.6 kHz at 800 eV . The ion distribution in these conditions shows a novel feature which is clear looking at the red curve in Fig.5: it is not anymore characterized by a linear trend and thus a constant global diffusion coefficient cannot be easily defined. The reason of this non-diffusive behavior can be understood by analyzing the pitch angle of the lost ions and of those closer to the last conserved helical surface (highest ψ^M values). We have reported the corresponding pitch angle distribution in Fig. 6 which shows that most of these lost ions are trapped with a pitch angle close to zero.

At very low collisionality (high temperatures) passing ions are affected only by the remnant chaos (by secondary modes) and from a small thermal drift due to their non-zero temperature; thus their transport is very low. This is shown in Fig. 6-(b) where transport simulations for only passing (black, $\lambda=0.7-0.9$) and only trapped ions (red, $\lambda=0-0.2$) have been performed at $T=800 \text{ eV}$.

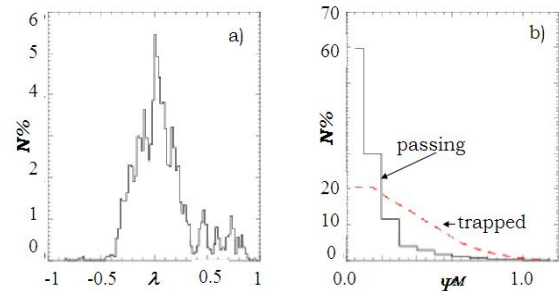


Fig.6 a) Pitch angle distribution of the escaping ions.

b) Simulation of transport in QSH for only trapped (red) and only passing ions (black).

Even in a very low collisionality regime trapped particles diffuse across the helical magnetic surfaces and their density distribution is almost linear. On the other hand, until the level of the secondary modes is low enough, passing particles follow the helical magnetic field lines inside the helical structure and perform many toroidal turns until a collision deflects them from their initial orbit. These simulations show that the ratio of the diffusion coefficients using only passing (D_{pas}) or trapped particles (D_{trap}) is about $D_{pas} / D_{trap} \sim 0.01$ at $T_e=T_i=800 \text{ eV}$ and

confirms that neoclassical effects become dominant when reducing collisionality. The values of D reported above have been obtained by the geometric average between the electron D_e and the ion diffusion D_i coefficients computed by the numerical simulations. This is performed in order to estimate the ambipolar effect within the helical structure as done in [17]. For a more detailed and correct evaluation of D , an electric field E should be implemented in the code to ensure the ambipolarity condition. Anyway, it must be noted that while in the pure SH case the electron D_e and ion D_i are quite different ($D_i/D_e \sim 5$), in the more realistic QSH scenario they are much closer each other (D_i/D_e in the range 1-2). In this latter case the electric field required should be very small and the ambipolarity constraint may provide only a mild impact.

As previously described, trapped particles inside a magnetic island can be both helically or poloidally trapped. The radial excursion of the guiding center position in a banana orbit is an increasing function of the ion thermal energy. While at a temperature of 300 eV its size is of the order of 0.5cm for hydrogen, it can reach also values between 2 and 5cm for T_i in the range 0.6-1.5 keV. Thus, few banana orbits are enough for an ion to drift out the helical structure. On the contrary, electrons are less affected by neoclassical effects: because of their low mass, banana orbits have a very small width (less than 1 mm in the radial direction, like in MH). Ion species with higher atomic mass A and electric charge Z are usually characterized by thinner banana orbits with respect to a hydrogen ion: the radial width excursion depends on the thermal velocity of the considered particle, which for a given energy E is proportional to $(EA)^{1/2}$. For example, an ion of OVII with $A=16$ has 1/4 of a hydrogen banana width for the same energy E . Experiments and numerical studies on impurity transport mechanisms in the helical structure are still in progress.

4. Conclusions

The contribution of particle trapping to various aspects of the RFP physics has been investigated in the paper. The trapped particle fraction in an axisymmetric RFP is almost the same as in a tokamak with the same aspect ratio. The banana width is typically comparable with the gyro-radius, with peculiar consequences on the actual weight of neoclassical effects on macroscopic quantities and phenomena: the bootstrap current remains negligible as compared to the tokamak case, while the resistivity turns out to be enhanced up to a factor 2 in the axisymmetric case. Further work will be done for the computation of such quantities in the Single Helicity configuration, where the *total fraction* of trapped particles increases up to ~40%, against the axisymmetric value ~30%. As far as particle transport is concerned,

particle trapping is found to have a strong influence especially in the QSH configuration; as proved, this is the foremost mechanism of transport across the helical structure at the rather low collisionality achieved in QSH-SHAX regimes of RFX-mod [21]. Indeed the neoclassical effect generates the main contribution to the average diffusion coefficient (which is presently estimated to be one order of magnitude larger than the classical contribution). On the other hand, due to the reduced level of magnetic chaos, passing particles are confined for a very long time along well conserved magnetic surfaces. Conversely, in the chaotic MH states, the neoclassical contribution to particle transport is largely overcome by passing particles, which participate to long-distance flights along the chaotic magnetic field lines [22].

Finally, we point out that, due to the significantly large fraction of trapped particles - locally very large in QSH-SHAX regimes - the instability of trapped electron modes (TEM) is likely to play a role in the transport for low chaos RFPs, which is a topic under investigation.

This work was supported by the European Communities under the contract of Association between Euratom/ENEA.

References

- [1] P. Sonato *et al.*, *Fus. Eng. Des.* **66**, 68 (2003)
- [2] R.B. White and M.S.Chance, *Phys. Fluids* **27**, 2455 (1984)
- [3] L. Guazzotto *et al.*, *Phys. Plasmas* **11**, 604 (2004)
- [4] R.B. White, *The Theory of Toroidally Confined Plasmas*, Imperial College Press, London (2005) p.88
- [5] M.R. Stoneking *et al.*, *Phys. Plasmas* **5**, 1004 (1998); J.K. Anderson *et al.*, *Nuclear Fusion* **44**, 162 (2004)
- [6] S. Shiina *et al.*, *Phys. Plasmas* **12**, 070802 (2005)
- [7] S. Cappello, *Plasma Phys. Contr. Fus.* **46**, B313 (2004)
- [8a,b] a) J.P. Freidberg, *Ideal Magnetohydrodynamics*, Plenum Press, NewYork (1987), b) J.P. Freidberg, *Plasma Physics and Fusion Energy*, Cambridge University Press 2007
- [9] M. Wakatani *et al.*, *Jour. Phys. Soc. Japan* **34**, 181 (1973)
- [10] P. Helander, D.J. Sigmar, *Collisional Transport in Magnetized Plasmas*, Cambridge (2002)
- [11] P. Zanca & D. Terranova, *Plasma Phys. Control. Fusion* **46**, 1115 (2004)
- [12] S.P. Hirshman, *Phys. Fluids* **31**, 3150 (1988)
- [13] O. Sauter *et al.*, *Phys. Plasmas* **6**, 2834 (1999)
- [14] O. Sauter *et al.*, *Phys. Plasmas* **9**, 5140 (2002)
- [15] W.A. Houlberg *et al.*, *Phys. Plasmas* **4**, 3230 (1997)
- [16] T. Bolzonella *et al.*, *EPS Conf.* 2008, Crete, P5.097
- [17] I.Predebon *et al* *Phys Rev Lett* **93**, 145001 (2004)
- [18] I. Predebon *et al*, *IEEE Trans. Plasma Science* **33**, 460 (2005)
- [19] H.E. Mynick, *Phys. Fluids* **26**, 1008 (1983)
- [20] M.Gobbin *et al.*, *Phys Plasmas* **14**, 072305 (2007)
- [21] R. Lorenzini *et al.*, *Phys. Rev. Lett.* **101**, 025005 (2008)
- [22] G. Spizzo, R. B. White and S. Cappello, *Phys. Plasmas* **14**, 102310 (2007)